Sentinel-3 radar altimetry for river monitoring - a catchment-scale evaluation of satellite water surface elevation from Sentinel-3A and Sentinel-3B

Cecile M. M. Kittel[1], Liguang Jiang[1], Christian Tøttrup[2], and Peter Bauer-Gottwein[1]

[1]Department of Environmental Engineering, Technical University of Denmark, Technical University of Denmark, Kgs. Lyngby, 2800, Denmark
[2]DHI-GRAS, Hørsholm, 2970, Denmark

Correspondence: Cecile M. M. Kittel (ceki@env.dtu.dk)

Abstract. Sentinel-3 is the first satellite altimetry mission to operate in Synthetic Aperture Radar (SAR) mode and in open-loop tracking mode nearly globally. Both features are expected to improve the ability of the altimeters to observe inland water bodies. In this study we evaluate the possibility to extract river water surface elevation (WSE) at catchment level from Sentinel-3A and Sentinel-3B radar altimetry, using Level-1b and Level-2 data from two public platforms. The objectives of

5   the study are to evaluate the density of valuable observations and establish a WSE monitoring network. Additionally, we demonstrate the potential application of Sentinel-3 for monitoring river interactions with wetlands and floodplains. In the Zambezi basin, 175 virtual stations (VS) contain useful WSE information in both datasets, far exceeding the number of VS available in standard databases. The RMSD is between 2.7 cm and 31.2 cm at six in-situ stations and the VS reflect the observed WSE climatology throughout the basin. Additional VS are available in both the Copernicus Open Access Hub and

10   GPOD (Grid Processing on Demand), highlighting the value of considering multiple processing options. In particular, we show that the processing options available on GPOD strongly affect the number of useful VS; in particular, extending the size of the receiving window, considerably improved data at 13 Sentinel-3 VS. The number of VS delivering usable data increased after the Open-Loop Tracking Command (OLTC) on board Sentinel-3A was updated. However, the open-loop tracking mode poses two new challenges: correct on board elevation information is crucial, and steep changes in the receiving window position can

15   have detrimental effects on the WSE observations. Finally, we extract Sentinel-3 observations over key wetlands in the Zambezi basin. We show that clear seasonal patterns are captured in the Sentinel-3 WSE, reflecting flooding events in the floodplains. These results highlight the potential of using Sentinel-3 as a SWOT (Surface Water and Ocean Topography) surrogate while awaiting the mission launch. The results show the benefit of the high-resolution Synthetic Aperture Radar (SAR) altimeter, as well as the benefits and disadvantages of the open-loop tracking mode.

20   1   Introduction

Reliable water monitoring data hold very high value for water science disciplines including hydrological modelling and engineering applications, such as operational forecasting, and planning/designing water resources infrastructure. However, the

last decades have seen a steady decline in available water monitoring information, particularly in Africa (Hannah et al., 2011; Vörösmarty et al., 2001). Water surface elevation (WSE) is an important quantity in hydrological applications and is tradition-
25 ally recorded using in-situ instruments. In the last over 25 years, satellite radar altimetry has provided an alternative source of WSE observations.

Satellite radar altimetry has been used to monitor water level and storage variations at regional scale (Arsen et al., 2015; Boergens et al., 2017; Jiang et al., 2017a; Kleinherenbrink et al., 2015; Villadsen et al., 2015), to assess river dynamics and estimate river discharge (Michailovsky et al., 2012; Roux et al., 2010; Tarpanelli et al., 2017), and to support hydrodynamic
30 modelling (Domeneghetti et al., 2014; Kittel et al., 2018; Michailovsky et al., 2013; Schneider et al., 2017). Water level observations are useful to constrain hydrologic/hydrodynamic model parameters. Getirana and Peters-Lidard (2013); Liu et al. (2015); Jiang et al. (2019b) all used altimetry WSE to calibrate hydrodynamic models. In Kittel et al. (2018), WSE from Envisat and Jason-2 was used to calibrate a rainfall-runoff model of the Ogooué River. The observations supplemented historical discharge records by providing contemporary observations of river levels, and were shown to help constrain the routing model
35 parameters in the poorly gauged catchment. Several databases provide global and publicly available time series of WSE for inland water bodies derived from satellite altimetry observations (Berry et al., 2005; Crétaux et al., 2011; Schwatke et al., 2015), including the operational database Hydroweb, which contains updated WSE time series from Sentinel-3 observations (Rosmorduc, 2016).

Advancements in instrument design and processing tools have steadily improved the accuracy of data products to the order
40 of decimeters (e.g. Vu et al. (2018); and Villadsen et al. (2016) for a summary of mission performance evaluations across the literature). In particular, Synthetic Aperture Radar (SAR) altimeters reduce the size of the along-track footprint and have improved the number of targets and potential accuracy in coastal areas and over inland water by reducing land contamination (Dinardo et al., 2018; Jiang et al., 2017b; Nielsen et al., 2017; Wingham et al., 2006).

The European Space Agency (ESA) Sentinel-3 mission is a marine and land mission currently operating in a two-satellite
45 constellation: Sentinel-3A and Sentinel-3B launched in February 2016 and April 2018 respectively. The satellites both carry dual-frequency (Ku- and C-band) Synthetic Aperture Radar Altimeters (SRAL) on board, building on the heritage of the CryoSat-2 and the Jason missions (Jiang et al., 2020). In Synthetic Aperture Radar (SAR) mode, the altimeter has a higher along-track resolution of 300m compared to 1.64 km in Low Resolution Mode (LRM). The instruments operate 100% in SAR mode between 60°N and 60°S, making Sentinel-3 the first satellite altimetry mission to provide near global coverage in SAR
50 mode.

The on board tracking mode of Sentinel-3 is different from the previous SAR altimetry mission CryoSat-2. The tracking mode determines how the range window is re-positioned as the satellite proceeds along its orbit. The positioning of the range window, which is 60 m wide, ensures that the return echo of the transmitted microwave pulse is correctly recorded by the altimeter. CryoSat-2 and SARAL/AltiKa both operate in closed-loop, that is the range window is positioned based on infor-
55 mation from previous measurements. However, if the satellite fails to correctly record the river echo, e.g. in steep river valleys where the satellite records the valley top instead of the valley bottom, the error will be transmitted to future measurements as the satellite locks on the wrong target. Studies have demonstrated this challenge for steep-river valleys, e.g. in France (Bian-

camaria et al., 2018) and in China (Jiang et al., 2017b). In open-loop mode, a priori information about the surface topography controls the range window position, in the form of an on board lookup table, the Open-Loop Tracking Command (OLTC) tables. Previous studies have demonstrated that Sentinel-3 is less affected by abrupt changes in topography, provided the on board elevation information is correct (Jiang et al., 2020, 2019a).

To allow continuation of the historical ERS/Envisat time series, the Sentinel-3 orbit is similar to the orbit of Envisat. At the equator, tracks are spaced 52 km apart, offering a high spatial density of potential virtual stations (VS) on rivers globally, with a return period of 27 days. A number of VS are already available from Sentinel-3A, based on the on board Hydrology Database (HDB) targets; however, a much higher number of VS are potentially available when considering all crossings between river centerlines and satellite ground tracks. For instance, there are over 300 potential Sentinel-3A VS in the Zambezi basin of which only 38 VS are available on Hydroweb (http://hydroweb.theia-land.fr/). Furthermore, the mission has operated in dual-satellite constellation since November 2018, providing at least one year of non-time critical data from Sentinel-3B.

The aim of this study is to assess the potential of the Sentinel-3 mission in hydrological applications (e.g. monitoring, modelling and river-floodplain interactions) by extracting a catchment-scale WSE monitoring network of Sentinel-3 VS. Where ground observations are available, we evaluate the satellite performance directly against in-situ data. We investigate the impact of processing choices, by evaluating the implications of the open-loop tracking mode and on board OLTC for hydrological applications. Finally, we explore the potential for spatio-temporal monitoring of wetlands and floodplains using Sentinel-3. The purpose of these investigations is to confirm that the network can serve as a useful supplement to the in-situ gauging stations by capturing temporal dynamics across the catchment.

To address these objectives, we extract all available Sentinel-3A and Sentinel-3B observations over the Zambezi basin using two publicly accessible databases. We present an automatically extracted catchment-scale river WSE monitoring network based on Sentinel-3 radar altimetry. All processing steps are performed on publicly accessible databases or using open-access code.

2 Data and study area

2.1 The Zambezi basin

The Zambezi basin is the largest river in Southern Africa and drains 1 390 000 km2 stretching over eight countries (Fig. 1). Water resources in the basin are crucial for human consumption, hydropower production, irrigation and ecosystem services (Beilfuss, 2012). There are three distinct seasons: the wet and warm season from November to April, the cool and dry season from May to July and the hot and dry season between August and October. The river and its tributaries display a strong seasonal signal, which should be reflected by the satellite altimetry dataset.
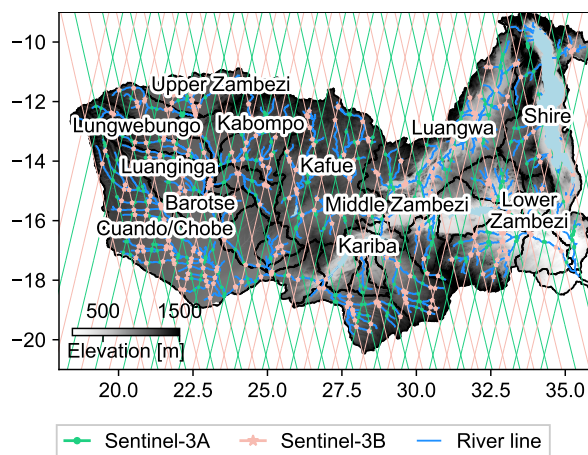
Figure 1. Base map of the study area. All Sentinel-3 tracks and river-track-crossings (VS) are shown for the entire Zambezi basin.

Previous studies have evaluated other altimetry missions over the Zambezi, providing a reference in terms of performance of new satellites (Michailovsky et al., 2012; Michailovsky and Bauer-Gottwein, 2014). As shown in Figure 1, satellite tracks cross the river and its tributaries at multiple locations, and several ground-tracks cross important wetlands (e.g. the Barotse floodplain, Chobe floodplain and the Kafue flats).

90   Water resources in the Zambezi River basin are increasingly subject to stress, as several drought episodes have affected Southern Africa in the last 30 years (Abiodun et al., 2019). Monitoring is key to adaptation and mitigation efforts. Remote sensing observations of WSE can provide useful monitoring information and inform forecasting and planning tools in poorly instrumented areas. The collection of consistent water level remains a challenge for the member states, especially in the upper parts of the Zambezi, where system failure and vandalism are a constant disruption of the existing ground monitoring system.

95   Thus, a WSE monitoring network based on altimetry observations could ensure steady information on water levels in the catchment even if the existing ground system is not in operation.

2.2 Auxiliary data

2.2.1 Virtual station localization

A virtual station is defined as the intersection between a river line and a satellite ground track. Each time the satellite returns on

100 the given pass, new observations of the river can be added to the WSE time series at the virtual station. The river line is from the open data set of global river networks from Yan et al. (2019), which is based on two DEMs (Digital Elevation Model): the SRTM (Shuttle Radar Topography Mission) and ASTER GDEM v.2 (Advanced Spaceborne Thermal Emission and Reflection Radiometer Global Digital Elevation Model) datasets at 90 m and 30 m resolutions respectively. The dataset was selected as it includes a stream burning step prior to the application of the river delineation algorithm, which is particularly useful for plain

areas. The burnt-in river line is obtained from Google Earth, using the highest possible image resolution and manually drawing the river line as close as possible to the centerline.

2.2.2 Water mask

To ensure that observations are over water, we use v.1.1 of the water occurrence maps from Pekel et al. (2016). The maps are based on 3 million satellite images from Landsat from 1984 to 2018 and indicate seasonal and annual changes in global surface water occurrence at 30-meter resolution. The occurrence map indicates the percentage occurrence of water. We use a threshold of 10% water occurrence frequency over the 34 years of record. A low threshold is chosen on purpose to ensure all valuable data, including seasonal water, is extracted at the cost of a higher outlier frequency. This ensures that data points are not masked out because of low water occurrence probability, which could be partly due to cloud cover.

2.2.3 Digital elevation model

We use the MERIT DEM (Multi-Error-Removed Improved-Terrain DEM) as reference surface elevation (Yamakazi et al., 2017). MERIT is based on widely used DEMs, including SRTM, which have been corrected for several error sources (speckle noise, tree height bias etc.). It is provided at 3sec resolution and referenced to the EGM96 geoid. We reproject the DEM onto the EGM2008 geoid using the VDatum software (Myers et al., 2007).

2.3 Sentinel-3 Level-1b and Level-2 data

Table 1 summarizes mission specifications for the Sentinel-3 satellites. Level-1b and Level-2 data for the area of interest are retrieved from 1) the ESA GPOD SARvatore (Grid Processing on Demand SAR Versatile Altimetric Toolkit for Ocean Research and Exploitation) service and 2) the Copernicus open access hub, SciHub. Both services are freely available upon registration and use the exact same Level-1a data for processing. With the exception of in-situ observations, none of the processing steps or data are catchment specific.

Table 1. Sentinel-3 mission specifications.

	Sentinel-3A	Sentinel-3B
Launch	16/02/2016	25/04/2018
Data coverage	01/06/2016 - present	01/11/2018 - present
Planned Lifespan	7 years	7 years
Elapsed lifespan	4 years	2 years
Orbit	Polar, sun-synchronous	
	27 day repeat cycle	
Ground track separation	104 km at the Equator	
	(52 km in two-satellite constellation)	
Instrument	Synthetic Aperture Radar Altimeter (SRAL)	
	Ku-band	
	(300 m resolution after SAR processing)	
Operating mode	Open-loop	
Footprint	300 x 1.64 km (along-track x across-track)	

125   The Level-1b data and Level-2 data are specific to the two databases. Both datasets contain the auxiliary data necessary to
compute the water surface elevation. In both datasets, geoid data is provided. Although both use the EGM2008 geoid model, the
geoid model parameters as well as the geophysical corrections can differ slightly. We observe a bias between the two datasets
of varying magnitude throughout the basin. Therefore, only the relative change in water surface elevation will be considered
when comparing the datasets.

130   **2.3.1   GPOD Processing**

A processing configuration tailored for inland water is available on GPOD. In particular, four specific options are applied
during processing (Dinardo et al., 2018):

–   A Hamming weighting window is applied on the burst data prior to the azimuth Fast Fourier Transform (FFT) to reduce
    the impact from off-nadir bright targets by reducing the side-lobes of the Delay-Doppler beam

135   –   A factor two oversampling of the radar waveform prior to the range FFT to improve sampling efficiency of peaky echoes
    from bright targets

–   An extension of the receiving window N times, to better accommodate the L1b echoes in the receiving window over
    rough topography.

A double or larger extension of the receiving window (N≤2) is recommended for regions with rapidly changing topography
140   (Dinardo et al., 2018). The standard fixed-size receiving window of 256 samples may not be able to store the full L1b echo and
may result in a truncation of the leading edge. This has been reported for satellites operating in closed-loop mode, where there

may be a transition phase before the window has been positioned correctly by the satellite. In open-loop mode, truncations are most likely to occur close to changes in the OLTC, where the receiving window may still be positioned according to the previous target. Inland water targets might be far apart, resulting in steep changes when a new target is introduced. We therefore
145 process all tracks using a double and triple receiving window, to identify where the extension might be useful. This window is not to be confused with the on board reception window, which determines when the altimeter records the return echo from the emitted pulse, and cannot be modified by on-ground processing. GPOD uses the Samosa+ retracker to retrieve the nadir range. Samosa+ is a physically-based retracker specifically dedicated to coastal regions and described in detail in Dinardo et al. (2018). The GPOD datasets are referred to as the "GPOD dataset" in the following sections, with 2x and 3x respectively
150 indicating the double and triple receiving window extension.

2.3.2 Copernicus Open Access Hub Processing

The Copernicus Open Access Hub (previously Sentinels Scientific Data Hub) provides Sentinel-3 SAR data at various processing levels, including Level-1b and Level-2. In the Level-1b dataset, the echo waveforms are provided, in "counts" and are therefore not directly comparable to the GPOD waveforms. In the level-2 dataset, several retrackers are used. Over land, the
155 empirical OCOG (Offset Center of Gravity) retracker is used (Jain, 2015). The resulting dataset is referred to as the "SciHub dataset" in the following sections.

2.3.3 Water Surface Elevation

In both datasets, the 20Hz retracked range, R_{unc}, must be corrected for a number of geophysical and propagation effects (i.e. pole tides, solid Earth tides, ionosphere, and dry and wet troposphere), summed into R_{geo} to obtain the corrected range, R_c
160 (Eq. 1).

$$R_c = R_{unc} - R_{geo} \tag{1}$$

The water surface elevation is the satellite's altitude, h, relative to the reference WGS84 ellipsoid minus the corrected satellite range. The final WSE, H_{WSE}, is projected onto the EGM2008 geoid, by subtracting the geoid height, H_{Geoid} (Eq. 2).

$$H_{WSE} = h - R_c - H_{geiod} \tag{2}$$

165 All variables are expressed in meters. The corrections are provided along with the retracked data in each respective dataset.

2.3.4 Data selection

First, we select observations less than 2 km from a virtual station. We filter the observations over the water occurrence mask. The along-track resolution is 300 m. Therefore, a buffer of one observation around each water body is allowed. The water mask is based on Landsat observations and thus sensitive to cloud cover. In order to avoid that valid observations over water
170 are discarded based on an unreliable water mask, observations with high maximum Range Integrated Power (RIP) ($> 10^{-13}$)

or a high backscatter coefficient (>30 dB) are also classified as water. The σ_0 threshold is set based on trial and error for the basin and previous studies (e.g. Michailovsky et al. (2012)).

This step also ensures that valid observations are not removed, in case smaller tributaries are not present in the water mask. The final outlier removal at this stage is based on digital elevation values using the ACE2 DEM included in the GPOD dataset, and the MERIT DEM for the SciHub dataset. Differences in height exceeding 30 m are considered as outliers.

2.3.5 Level-1b waveforms

To evaluate and summarize the Level 1b waveforms, we calculate the following parameters (Jiang et al., 2020):

- Stack Peakiness (SP): ratio between the maximum fitted RIP and sum of fitted RIP

- Maximum Power (MP): maximum value of a waveform

- Pulse Peakiness (PP): ratio between maximum power and the sum of the waveform

- Number of peaks (NP): number of peaks in a waveform – a peak is defined as exceeding 25% of the MP (Jiang et al., 2020)

MP and NP are indicators of the presence and number of bright targets respectively, while SP and PP provide information on the shape of the waveform. A river-like surface is typically smooth and highly reflective, resulting in quasi-specular reflections. This will typically translate into narrow, peaky waveforms and consequently high SP and PP values. The parameters are useful when comparing effects of the OLTC update for Sentinel-3A as well as processing parameters for both satellites.

In order to evaluate the open-loop mode, we use the tracker range. The tracker range is the on board positioning of the expected leading edge according to the OLTC. On Sentinel-3, the tracker range is positioned at bin 43 (counting from 0), one-third of the full window. The positioning of the window is done through the so-called window delay, or the delay between the pulse emission and the time of record of the tracker range. The epoch is the distance between the tracker range and the retracking position after L2 processing. The GPOD dataset contains the epoch (in m), which can be converted to number of bins and used to extract the retracking position. Repositioning to the center of the original reception window requires taking into account 1) oversampling and 2) the receiving window extension (2 x or 3 x), as described in 2.3.1. The tracker range (in m, referenced to bin 43, the nominal tracking position) is directly provided in the enhanced measurement file from SciHub.

Retrieving the untracked range gives an assessment of whether the expected WSE was within the on board reception window, meaning whether any useful data will be retrievable or not. Furthermore, it provides insight into the behavior of the two datasets at virtual stations close to sharp changes in the reception window positioning. Finally, the retracking position indicates whether the range was correctly retracked, when compared to the waveform.

2.3.6 Level-2 WSE

All observations retained at a given virtual station are processed to produce a WSE time series. A backscatter coefficient threshold of 30 dB ensures that only observations of bright targets (such as water) are included in the final selection used to produce WSE time series at each VS.

Level observations from 14 operational gauging stations were kindly provided by the Zambezi River Authority (ZRA), who maintain the dataset. Six of the in-situ gauging stations were in sufficient proximity to a Sentinel-3 virtual station (< 20 km) and located on the same stream, and therefore suitable for direct comparison. Furthermore, we verify that the catchment area is sufficiently similar between the in-situ and virtual stations to justify comparison (e.g. no major tributaries between the two stations). The contributing areas differ by less than 5.5% in all cases. At all selected stations the level records were labelled as "Very good quality" and provided at daily temporal resolution, with an accuracy of 1 mm.

In order to account for any vertical bias between the two datasets, the mean level at overlapping sensing dates is subtracted from the in-situ and satellite WSE respectively. Performance is evaluated by calculating the RMSD (Root Mean Square Deviation) between the relative in-situ (w_g) and satellite (w_s) levels (Eq. 3), and the WRMSD (Weighted RMSD) by dividing with the residuals with the in-situ standard deviation.

$$D_{RMS} = \sqrt{\frac{1}{N}\sum_{i=1}^{N}(w_{g,i} - w_{s,i})^2} \tag{3}$$

Based on past mission performance as summarized in Villadsen et al. (2016), RMSD values below 30 cm are considered good, between 30 and 60 cm are considered moderate. We calculate Pearson's correlation coefficient to evaluate the linear correlation between the in-situ and remote sensing WSE. The correlation coefficient should be above 0.9. We correct for datum shifts by using the WSE amplitude and therefore expect a bias of 0 cm.

Additionally, historical records from 2000-2010 were available at 12 additional gauging stations. Although the stations could not be used directly due to the lack of temporal overlap, they can still support a visual assessment of the annual water level variations recorded by Sentinel-3. At ten stations, the in-situ station and Sentinel-3 VS were located on the same stream and within close enough proximity to be representative of similar catchment areas.

3 Results

The Sentinel-3 VS in the Zambezi are shown in Fig. 2. The percentage of missing data is calculated as the number of days with WSE observations divided by the number of days the satellite passed over the VS. There are 80 VS for Sentinel-3A and 101 VS for Sentinel-3B with complete WSE time series in both the GPOD and SciHub datasets (< 20% missing data). The rejection rate is slightly higher when using the GPOD dataset than when using the SciHub dataset (respectively 54% and 50% for Sentinel-3B and 35% and 31% for Sentinel-3A). This difference can be attributed to the higher proportion of no-data values and the generally lower σ_0 values in the GPOD dataset. The higher percentage of no-data values is due to the nature of the Samosa+ retracker: it is a physically based model and more sensitive to erroneous waveforms than the empirical OCOG

230   retracker. The lower backscatter values are related to the L1b processing and how the waveform is derived. σ_0 is inherently

related to the L1b processing and will be different in two the datasets. Generally, σ_0 is around 30% higher in the SciHub

dataset. We use the same threshold because the intention is to remove obvious non-water targets. Increasing the threshold for

the OCOG dataset did not improve outlier filtering as clearly defined non-water targets still had much lower σ_0 values, and

some SciHub observations with very high backscatter values were clearly not valid observations of water level (high standard

235   deviation within the selected pass, no consistent seasonal pattern, poor L1b statistics etc.).

    We note that 30 VS have valid data only after the OLTC update of Sentinel-3A in March 2019. At 25 VS, extending the

receiving window by a factor of three rather than two, increases the data coverage in the GPOD processing workflow. These

VS are considered separately in the following sections. In general, the valid VS are predominantly located on higher level

branches and tributaries of the basin and close to or on floodplains (Fig. 2). These targets are generally wider, perennial and the

240   topography flatter. Conversely, several rejected VS are located in the headwater subcatchments on smaller tributaries. Although

missing data represents less than 20%, the data is not necessarily useful and further analysis is required to evaluate the quality

of the WSE observations at the VS properly.
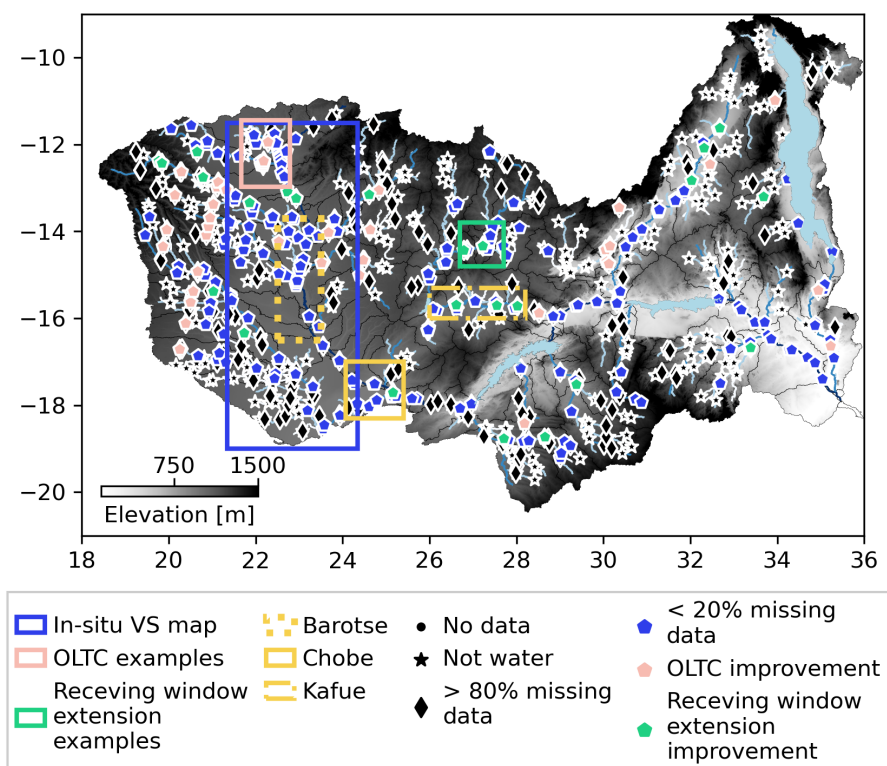
Figure 2. Zambezi Sentinel-3A and 3B VS after outlier filtering. Stations which improved by modifying processing steps (either on board through the OLTC update or on-ground by extending the receiving window on GPOD) are highlighted separately. The frames indicate examples highlighted in the next sections of this study. Additional maps are included in the supplementary material (Fig. A1, B1, and C1).

3.1 L1b at selected VS

The first step in validating the selected VS is to evaluate whether observations are over water. To assess this, we evaluate the

245 L1b data (Fig. 3 and Table 2). In the GPOD dataset, a high percentage of the VS have high PP and SP values (respectively above 0.1 and 0.2) combined with single peak waveforms (NP = 1) and high power (MP > 1e-15 in Watts). High SP and PP values indicate a quasi-specular reflection, consistent with river surfaces, while unique peaks and high power indicate low contamination from surrounding bright targets. We see in Fig. 3 that the bulk of the rejected waveforms are rejected because of the NP criterion. A number of VS might have high PP and SP values but contaminated waveforms, likely due to nearby bright

250 targets. As the SP and PP cannot be calculated based on the waveforms processed on SciHub, we use NP alone as the L1b selection criterion. We see that the L1b selection process counterbalances the lower rejection rate in the SciHub dataset.
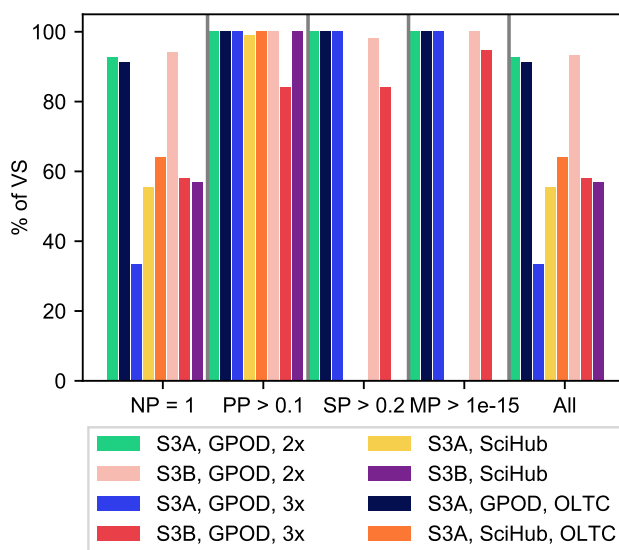
Figure 3. Stations fulfilling the L1b selection criteria in percentage of VS selected based on L2 data. Note that ESA SciHub does not provide the waveform in power; therefore, SP and MP are not calculated and are not part of the "all criteria fulfilled" evaluation.

The VS with valid Level 2 WSE time series but invalid waveform statistics from the GPOD datasets are spread throughout the catchment with most stations on Luangwa and on the Lower Zambezi (both S3A and S3B) and on the Kafue (S3A). The rejection rate is higher in the SciHub dataset, with rejected stations throughout the basin.

Table 2. Number of VS fulfilling criteria on Level-1b and Level-2 (% of VS retained) in the SciHub and GPOD datasets using the OCOG and Samosa+ retrackers respectively. We consider S3A VS with data only after the OLTC update as well as the two processing settings on GPOD (2x and 3x window extension) separately.

	GPOD		SciHub		Both	
	L2	L1b	L2	L1b	L2	L1b
Sentinel-3A						
2x extension	81	75 (93%)	108	60 (56%)	80	49 (61%)
3x extension	6	2 (33%)	-	-	6	0 (0%)
OLTC	34	31 (91%)	39	25 (64%)	30	24 (80%)
Sentinel-3B						
2x extension	103	96 (93%)	139	79 (57%)	101	66 (65%)
3x extension	19	11 (58%)	-	-	18	6 (33%)

255 Fig. 4 shows the L1b statistics at the VS where data improved after the OLTC update or by extending the receiving window on the GPOD processing platform. The post-update statistics are shown with the 3x receiving window extension for the GPOD dataset. Several Sentinel-3A VS had no data at all prior to the OLTC update. The GPOD dataset has more stations with NP > 1 after the OLTC update than the SciHub dataset. The waveform statistics suggest that using a dedicated processing setup such as the one on GPOD is beneficial; however, the correct options must be applied to achieve optimal results.

260 It is interesting to note that a high number of VS that were improved by extending the receiving window, are rejected based on the waveform criteria. Extending the receiving window ensures that the leading edge of the L1b echo is preserved. This is an advantage at VS where topography changes abruptly, as the full return echo can be contained in the receiving window from all beams used during multi-looking. However, it also increases the likelihood of including contamination from other bright targets, increasing the number of significant peaks in the waveform.
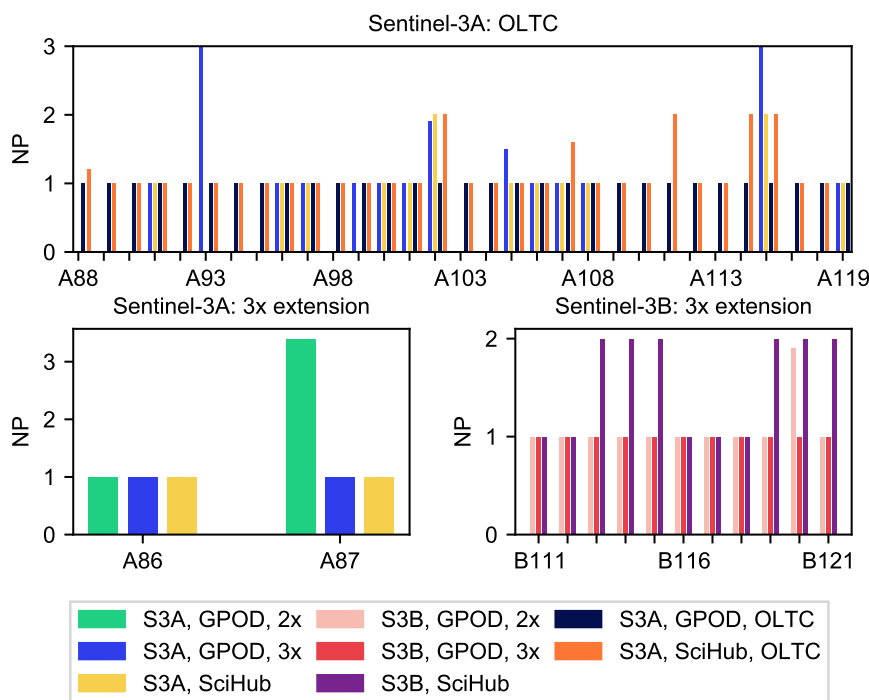
Figure 4. Number of peaks (NP) in waveform at stations improved by the OLTC update and by the 3x bin extension using GPOD processing. See the additional material for localization of the VS shown in the plot.

3.2 OLTC tables

The OLTC contains targets based on elevation information from hydrology databases (e.g. Hydroweb), virtual stations networks and the global ACE2 DEM (Altimeter Corrected Elevations v.2 Digital Elevation Model). The Sentinel-3A OLTC was updated in March 2019 with additional information for inland water targets. In total, there are over 80 new targets over the Zambezi River from hydrology databases represented in the new OLTC, compared to only two in version 4.2. In version 4.2, 64 targets were defined at ground track -river crossings and assigned ACE2 heights. These targets have also been updated with refined elevation information in OLTC version 5 to improve spatial coverage. The OLTC update introduced several new VS, which had no useful information prior to the update. Most new VS are located in the Upper Zambezi, where there were fewer targets in version 4.2. Only VS validated at Level 1b and Level 2 are included in Table 3. The number of VS consistently exceeds the number of targets, which is to be expected for plane areas, where even a single target may be sufficient to correctly track the WSE at multiple nearby crossing points.

Table 3. OLTC targets before and after March 2019 for the Zambezi catchment and their source (ACE-2 – global DEM or hydrology databases, HDB) – the targets are obtained from https://www.altimetry-hydro.eu/. The numbers in parenthesis are the Hydroweb Theia S3A VS available within each watershed (http://hydroweb.theia-land.fr/). The VS are grouped by major watersheds

	S3A						S3B		
OLTC Version	v. 4.2	v. 5	Number of VS				v. 2	Number of VS	
	ACE2	HDB	HDB	GPOD		SciHub		HDB	GPOD	SciHub
Upper Zambezi and Luena	0	0	6	11 (1)	4	0	6	3	8	21	1	13
Kabompo	0	0	3	4 (3)	3	0	2	2	2	1	0	1
Lungwebungo	3	0	7	13 (3)	8	0	9	7	8	10	2	8
Luanginga	0	0	0	11 (0)	3	0	11	3	0	5	0	3
Cuando/Chobe	1	0	2	18 (4)	6	0	15	5	3	21	2	18
Barotse	5	0	5	6 (5)	3	0	5	2	18	11	1	10
Middle Zambezi (Kariba)	15	1	9	2 (0)	0	0	2	0	12	4	1	2
Kafue	7	0	17	18 (14)	0	1	16	0	14	15	2	10
Mupato	2	0	3	3 (2)	0	0	2	0	4	2	0	1
Luangwa	4	0	9	8 (6)	3	0	7	2	6	4	1	3
Lower Zambezi (Tete)	25	1	20	8 (8)	0	1	7	0	33	8	0	3
Shire	2	0	6	6 (2)	1	0	3	1	7	3	1	3

3.3 WSE Evaluation

3.3.1 Validation at in-situ stations

The retracked WSE data are compared to the in-situ gauge levels at six locations in the basin; where VS and in-situ stations are sufficiently close geographically (Fig. 5). In all six cases, the twice-extended receiving window is sufficient and no new targets 280 were uploaded to the OLTC in March 2019 near the two S3A VS.
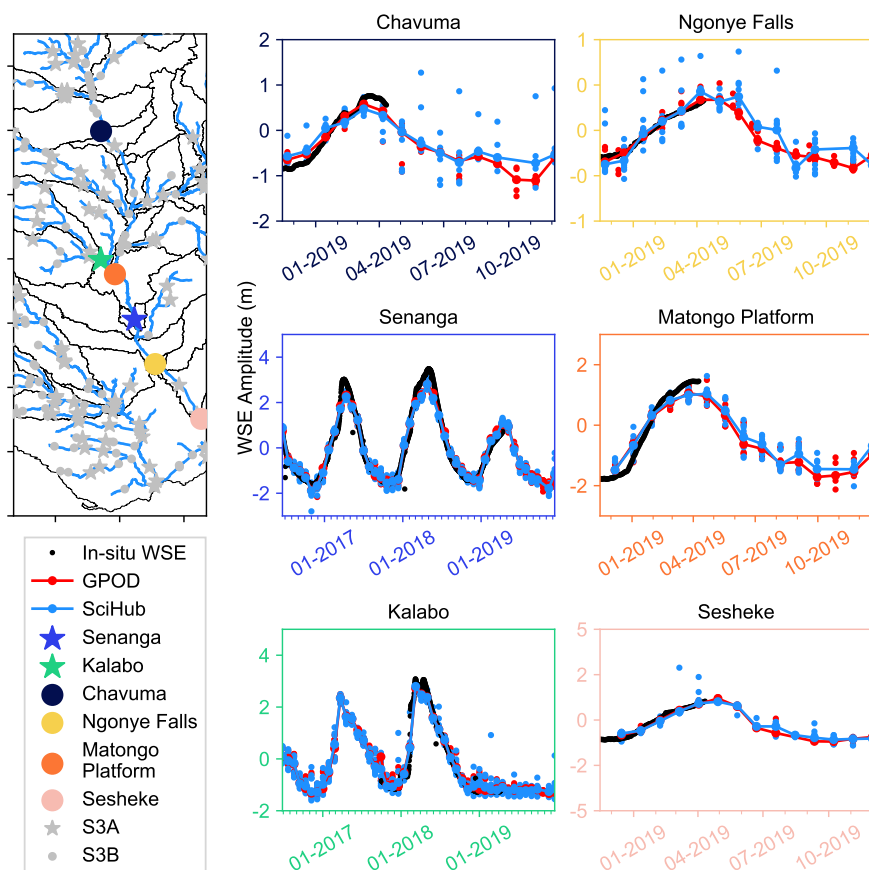
Figure 5. In-situ and satellite WSE at six locations in the Upper Zambezi basin. The plot colors correspond to the marker colors for each station in the map.

Performance at all six stations is highly satisfactory, based on visual inspection, performance statistics and in comparison to performance reported in past studies (Villadsen et al., 2016). The RMSD between the in-situ and satellite relative river levels is below 30 cm at five out of six stations, only the Matongo Platform has a moderate RMSD of 32 cm (Table 4). The largest RMSD are seen for the two VS furthest away from the closest in-situ gauge (19.3 km for Senanga and 15.8 km for the Matongo

285 platform). The systematic deviations between the in-situ and satellite WSE is to be expected given the long distance. For the remaining four stations, the RMSD is less than 15 cm with the Samosa+ retracker. Michailovsky et al. (2012) obtained RMSD between 24 and 106 cm at Envisat VS in the Zambezi catchment. The improvement in performance is consistent with the instrumental improvement between the two missions. Furthermore, the Samosa+ retracker outperforms the OGOC retracker at all stations except Matongo Platform, where the OCOG retracker improves the RMSD by 1.3 cm.

290 The WRMSD from the GPOD dataset varies between 4.4% and 18.9% of the in-situ standard deviation (Table 4). Thus, the error represents less than 20% of the variation in water level expected at each given location. The error is equivalent

to 1.3-6.3% of the mean annual amplitude. This confirms a low degree of uncertainty relative to the seasonal water level amplitudes. A closer look at the seasonal deviations provides additional insight into the uncertainty. As expected from Fig. 5, the underestimation of the peak water level is the main source of error at Senanga and Kalabo, whereas the error is similar across seasons at Ngonye Falls and Chavuma, and larger in the dry season at Sesheke and Matongo Platform.

Table 4. Performance statistics compared to neighboring in-situ gauge stations using S. Samosa+ on GPOD and O. the OCOG retracker from SciHub, to retrack satellite WSE. The relative RMSD is given in percent of the in-situ standard deviation.

In-situ station	VS platform	Distance to VS [km]	River width [m]	RMSD [cm] (% of the mean annual amplitude)	Dry season RMSD [cm]	Wet season RMSD [cm]	Relative RMSD [%]	r^2
Senanga	S3A	19.3	260	S. 25.8 (5.4)	15.2	36.4	17.9	0.987
				O. 28.1 (5.9)	16.0	39.6	19.6	0.985
Kalabo	S3A	4.8	35-600 (floodplain)	S. 13.6 (3.1)	8.6	18.8	9.4	0.998
				O. 15.1 (3.4)	11.4	18.6	10.4	0.998
Ngonye Falls	S3B	1.7	1100	S. 2.7 (1.3)	3.0	2.2	4.4	0.998
				O. 7.2 (5.3)	7.0	7.3	12.0	0.992
Chavuma	S3B	7.6	210	S. 15.8 (3.3)	15.9	15.7	11.9	0.997
				O. 25.6 (3.6)	25.4	25.9	19.3	0.979
Matongo Platform	S3B	15.8	95	S. 31.2 (6.3)	35.3	28.2	18.9	0.990
				O. 29.9 (6.0)	32.0	28.4	18.1	0.992
Sesheke	S3B	2.7	430	S. 10.5 (1.7)	13.6	7.8	5.4	0.991
				O. 14.7 (2.5)	19.2	12.2	7.5	0.978

3.3.2 Evaluation of hydrological pattern at catchment level

In-situ water level observations are available at ten other locations, where records end in the 2000s. As there is no overlap between the in-situ and VS time series, the stations cannot be used to quantitatively validate the nearest virtual stations. Instead, we visualize the annual water level variations to evaluate whether the time series appear coherent with the expected hydrologic patterns (Fig. 6).

In general, the patterns at several stations are coherent with the annual hydrological cycle observed in the corresponding region over the last two decades. The WSE observed by the satellite corresponds well with the amplitudes recorded at the gauging stations. The satellite time series appear smoother (e.g. at stations 3045, 5940 and 5099). This is logical as the 27-day return period increases the risk of missing the peak or low flow compared to a daily gauging record. We do note some obvious outliers, e.g. at station 1950, in the Sentinel-3A time series.
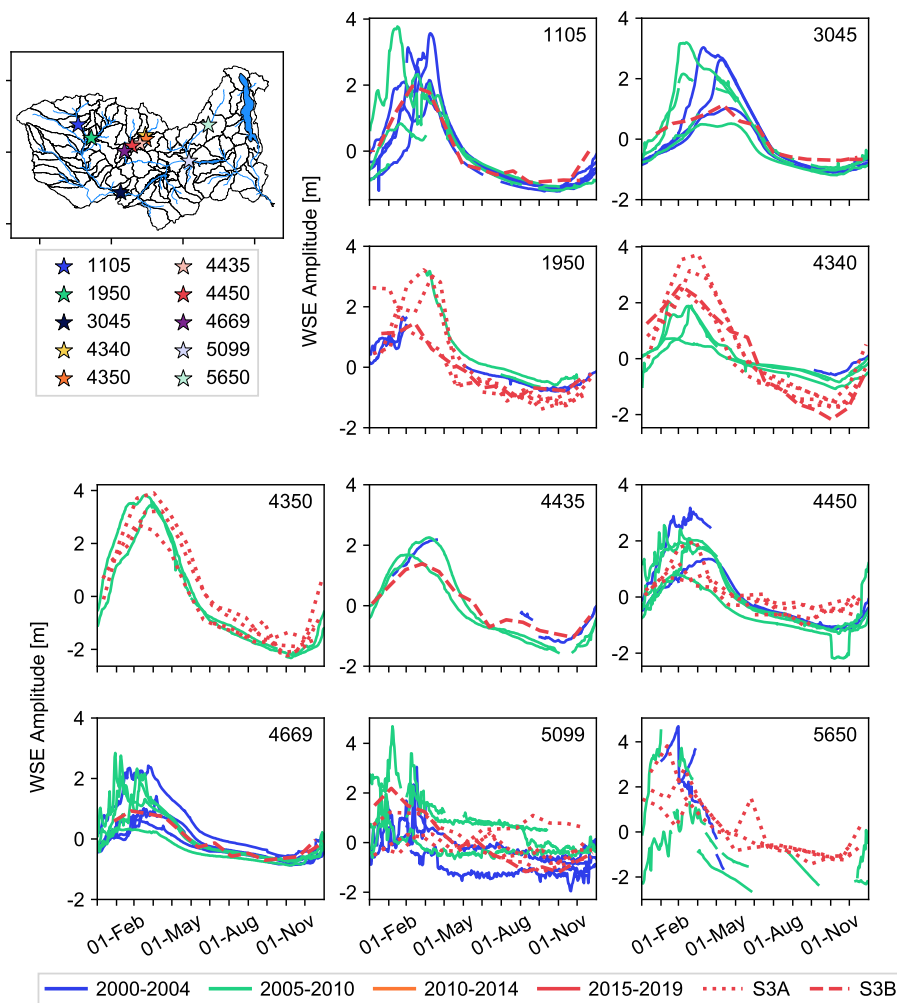
Figure 6. Comparison between in-situ annual WSE and satellite WSE at ten VS in the Zambezi basin. The colors indicate the time of observation. All elevations are referenced to the long-term average WSE to avoid bias due to the vertical datum. Stations 4340-4669 are all located on the Kafue in close proximity.

3.3.3 Annual amplitude of WSE

Fig. 7 shows boxplots of all useful VS based on the evaluation of the L1b and L2 data. The boxes delimit the IQR (Inter-Quartile Range – or between the first and third quartiles, Q_{75} and Q_{25} respectively) and the whiskers extend from $Q_{25} - 1.5 \times IQR$ to $Q_{25} + 1.5 \times IQR$. The amplitude within the whiskers varies between 1 m and 8.3 m. A closer look at the WSE recorded at the selected VS reveals a large number of extreme values in the initial dataset (Fig. 7, a). Even after outlier removal, there are still stations with very large amplitudes (> 20 m), which, based on the overall basin statistics, is unlikely. There are outlier removal approaches, which could be used to address this issue (e.g. IQR outlier removal, where points outside of the boxplot

whiskers would be removed); however, in several cases the filtering also removes peak annual discharge. In some cases, the 3x window extension reduces this amplitude, as does the OLTC update. At other stations, the amplitude increases with the

315   temporal coverage and data volume. If we consider the stations, which are valid across datasets, there are 145 Sentinel-3 VS in the Zambezi, which contain valuable information about WSE. The number of VS is quadrupled compared to using the global database Hydroweb.
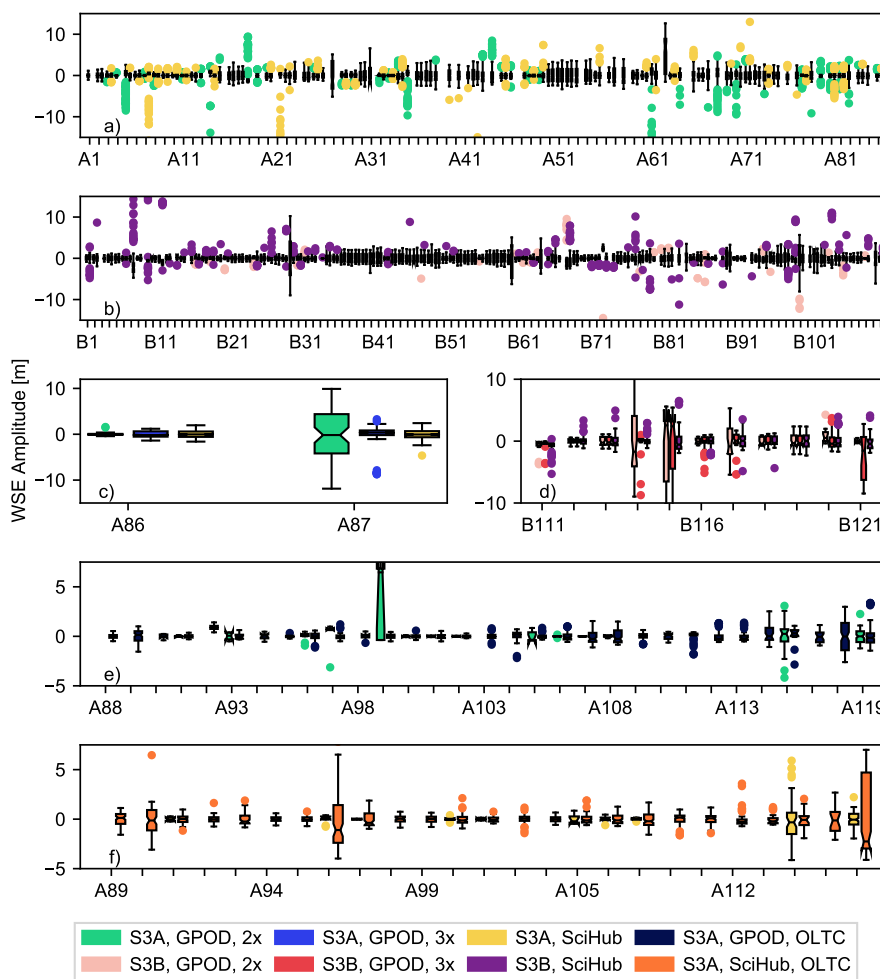
Figure 7. Boxplots of valid WSE for each VS (along the x-axis): a) all S3A VS, b) all S3B VS, c) S3A VS improved with the 3x receiving window extension, d) S3B VS improved with the 3x receiving window extension, and e) and f) S3A VS with observations after OLTC update only in the GPOD dataset and SciHub datasets respectively. The points are WSE outside of 1.5 times the InterQuartile Range (IQR), a common measure to identify outliers, to improve readability; the extreme outliers are cropped out of the plots. See Appendix for coordinates of the VS.

4 Discussion

4.1 Open-loop mode

320 At four stations in the Upper Zambezi, there are no valid observations at any of the VS prior to the OLTC update (Fig. 8).
These stations are good examples that illustrate the value of an up to date and precise OLTC to fully benefit from the open-loop
mode. We note that SciHub points are more scattered than the GPOD points, although the final time series is similar. The four
VS are amongst the VS which are unavailable on global river WSE databases from radar altimetry (e.g. Hydroweb, DAHITI),
illustrating the benefit of the proposed workflow to fully exploit the Sentinel-3 dataset at catchment level.
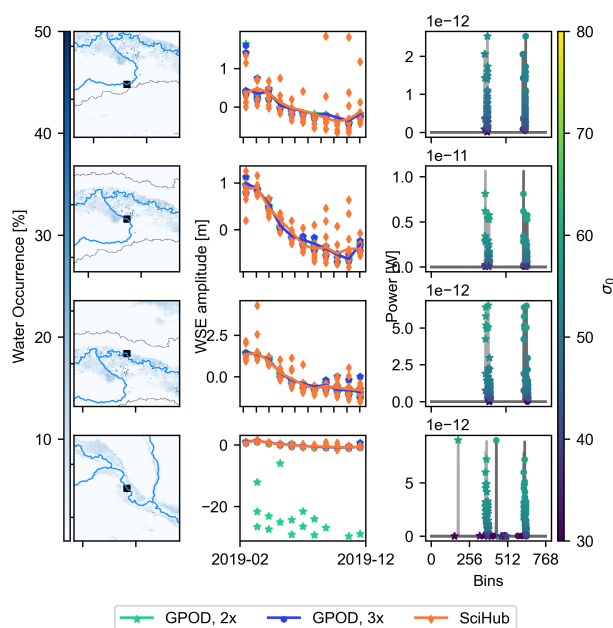
Figure 8. WSE time series in the Upper Zambezi and GPOD waveforms after the OLTC update. For clarity, we only show the GPOD
waveforms, as the conclusions are not affected by the L1b processing in any of these cases. Due to the window extension and padding of the
Hamming window on GPOD, the waveforms are shifted by respectively 256 and 512 bins for the double and triple extensions respectively.

325 Although the WSE time series are almost identical, Fig. 8 reveals several outliers at the last VS when using the standard
GPOD processing options for inland water. This is caused by incorrect retracking (points on the y = 0 axis in the waveform
subplot) and erroneous heights (WSE 10 to 20 m below the mean WSE). At the three other VS, increasing the window extension
factor has no effect.

Fig. 9 illustrates the stack waveforms for the last track before and after the OLTC update and the positioning of the altimeter
330 reception window. Before, the power was six orders of magnitude lower and the resulting WSE was 400 m below the DEM
elevation. The bright water target is clearly visible in the stack waveform after the OLTC update, whereas the waveform prior
to the update is clearly just noise. A closer look at the tracker range clearly indicates the discrepancy between the on board

elevation information and the actual surface elevation (Fig. 9). Furthermore, changes in the on board DEM introduce sharp transitions in the reception window, mimicking the effect of steep topographical changes, even in relatively flat regions. The

335   short closed-loop transition during the OLTC update reveals that this is exactly the case at the target. Therefore, processing decisions cannot be based on the topography alone but should take into account the on board information as well.
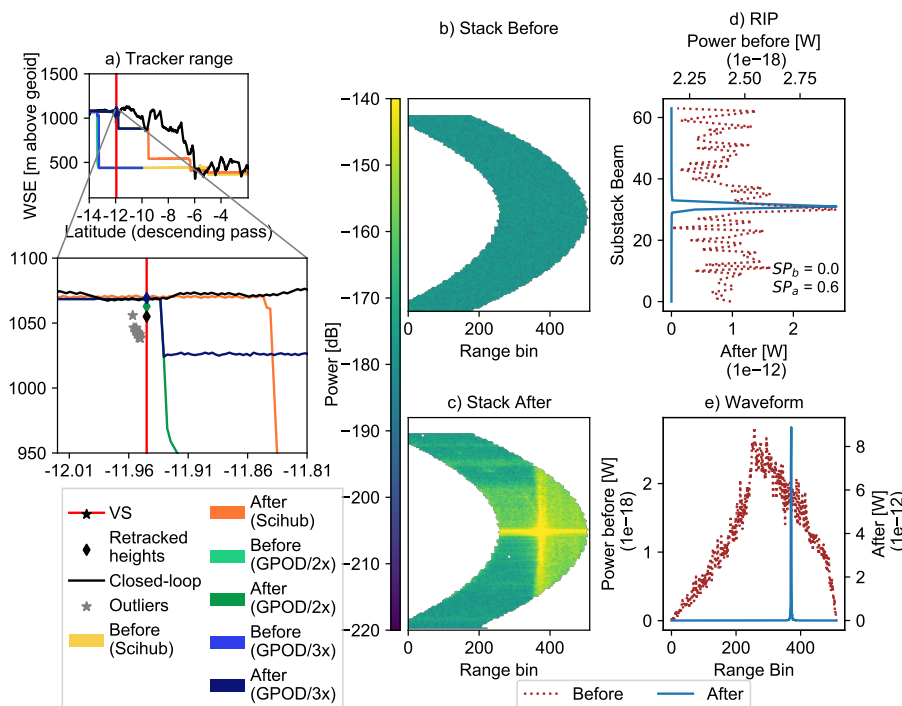
Figure 9. L1b data at VS on ground track 135 (descending path). a) Tracker range before, during and after the OLTC update and outliers using GPOD dataset with double window extension, b)-e) waveform statistics – the waveforms have been processed on GPOD: b) and c) stack waveforms d) Range Integrated Power (RIP) and e) waveforms before and after the Sentinel-3A OLTC update.

The maximum RIP and backscatter coefficients are equivalent for the two setups and the only difference is in the waveform misfit. The data does not offer insight into why the retracker fails at this location. The time series at this location does indicate that the triple extension may be more robust. Sentinel-3A briefly operated in closed-loop during the update period, between

340   1st of March 2019 and 9th of March 2019. Fig. 9 shows the tracker range during the update in black. The closed-loop mode performs very well and appears to capture changes in topography left out because of memory limitations imposed on the OLTC. This example illustrates that the benefit from open-loop over closed-loop tracking mode is clearly limited to VS where adequate elevation data is available in the OLTC. There is a risk of loss of data if the OLTC is not precise or dense enough. In that case, closed-loop mode may be preferable, particularly where topography does not change too abruptly.

4.2 Waveform processing - GPOD versus baseline processing

The L1b processing steps to generate the waveforms are different on GPOD and SciHub, and at some VS, this has clear consequences. Although the OLTC update has increased the number of VS in the Zambezi by 24 across datasets, we observe cases where the double extension dataset only contains data after the update, whereas extending the receiving window or using the baseline processing from SciHub yields valid data. We consider a virtual station on the Kafue at 1116 mamsl elevation. According to the OLTC website, there was no target near the VS prior to the OLTC update and the reception window was positioned at 978 mamsl based on the previous target. The reception window is more than 30 m below the target and the satellite should not have sensed the VS prior to March 2019. However, the tracker range from the SciHub dataset suggests that the window was actually positioned at around 1111 mamsl; therefore, the discrepancy must be related to the waveform processing, as illustrated in Fig. 10. After the OLTC update a target is defined for the VS at 1113 mamsl and the transition occurs earlier on the pass. The altimeter reception window has shifted just enough that the VS elevation is within the receiving window for all three datasets, including the GPOD dataset with the double extended receiving window.
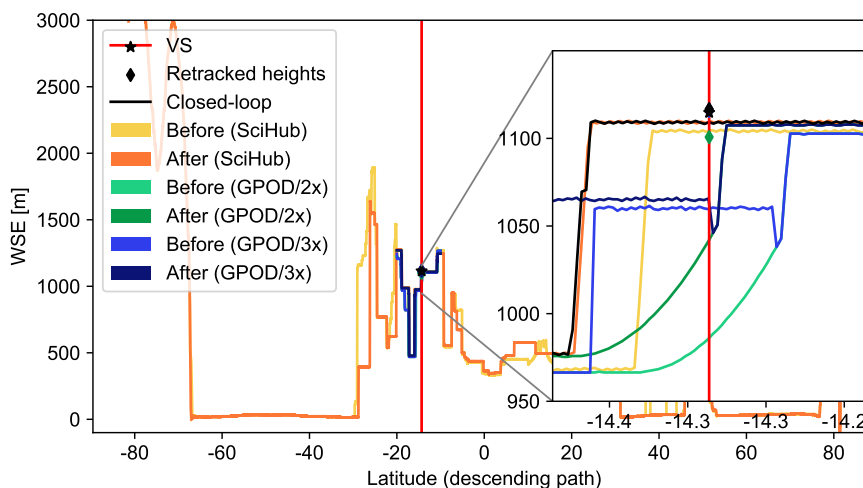
Figure 10. Tracker range for the three possible processing setups before and after the OLTC update.

The standard processing produces an abrupt change in the tracker range, consistent with the Sentinel-3 operating mode, where a target is retained until a new one is defined. If we consider the standard GPOD processing, the transition between two targets is smoothed. When the window is increased, the L1b echoes leading edge is preserved (Dinardo et al., 2018). This creates a stepwise transition (Fig. 10). A smoother transition may be an advantage for closed-loop processing, as demonstrated in Dinardo et al. (2018), however in open-loop processing, where the targets are immediately known, an unnecessary delay is introduced and the window extension becomes necessary to mitigate this.

Fig. 11 shows the waveforms and WSE time series at the station. The consequences of the different tracker range is clear: using the OCOG retracker and the standard SciHub dataset successfully produces a WSE time series with a clear seasonal

365 pattern. When using the GPOD dataset, a 3x extension of the receiving window is necessary to obtain data at this particular VS.
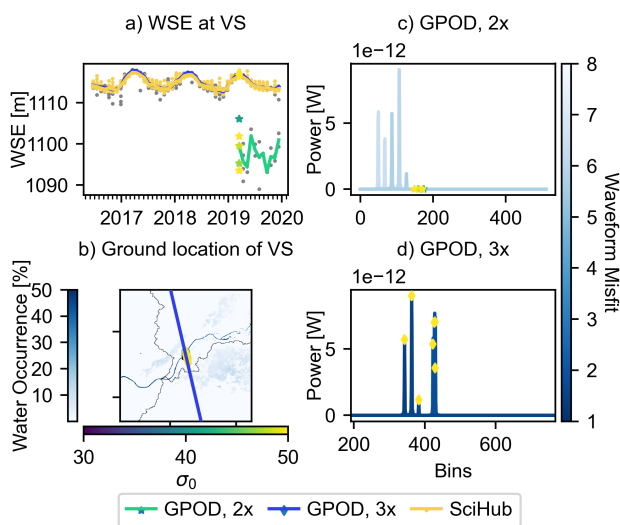
Figure 11. Comparison of WSE time series (a) and waveforms (c and d) at the VS on the Kafue (b) using the GPOD dataset with the Samosa+ retracker applying a double (c) and triple (d) extension of the receiving window and the SciHub dataset. The misfit parameter is provided with the GPOD dataset and is a measure of fit of the waveform model from the Samosa+ retracker to the actual model.

The effect of the pseudo-DEM is akin to that of sharp changes in elevation in coastal or mountainous areas for closed-loop operations (Dinardo et al., 2018). Abrupt changes in topography – or too far apart targets – can cause truncations in the waveform leading edge due to erroneous positioning in time of the radar's reception window. The options to mitigate include

370 extending the receiving window and thus making sure that the full echo can fit in the receiving window and that the leading edge is preserved (Dinardo et al., 2018) or ensuring that the target is defined early enough on the track to avoid consequences for the dataset.

4.3 River-floodplain interaction

The Zambezi is intrinsically linked to several significant wetlands, e.g. the Barotse floodplain, Kafue Flats and Chobe flood-

375 plain. At some VS, the WSE will reflect the river-floodplain interaction. Fig. 12 is an example from an S3B VS in the Barotse floodplain. The crossing tracks are both close to the river. The ascending track directly crosses the river, the waveforms and backscatter coefficients closely support a good target. We do see multiple peaks in the waveform as the target nears the edge of the river. The other track crosses the floodplain. When considering the two tracks separately, the interaction is clearly visible: the river level rises until it reaches the floodplain level. Subsequently, the river floods and water levels in the floodplain increase,

380 before decreasing again after the wet season. The river level decreases further to its original level, 1.5 m below the floodplain. The coupling is particularly visible during the flood recession phase, the early increase of the floodplain begins before the river reaches the floodplain level. It is unclear whether this is due to the local topography or to artifacts due to the track orientation.
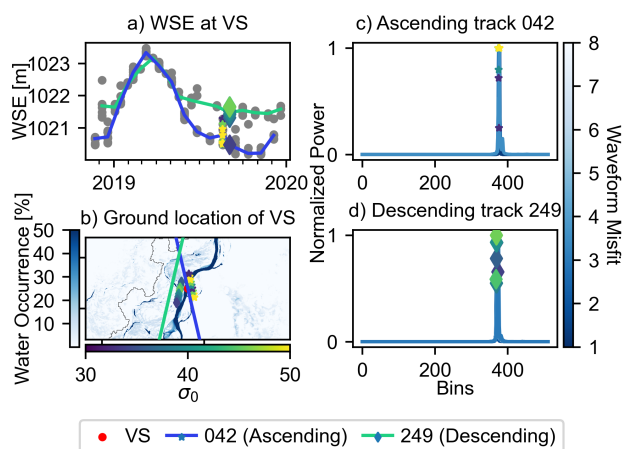
Figure 12. Demonstration of river-floodplain interactions at a VS on the Barotse floodplain. a) WSE at VS with highlighted observations showed in b) along with the water extent map and ground tracks, c) and d) waveforms from the observations from the two respective passes. The observations plotted are the same in a-d to illustrate the different data dimensions (ground location, WSE and backscatter coefficient).

The findings in Fig. 12 motivated an analysis of entire tracks crossing the floodplains. Rather than grouping by coordinates, we here assess specific relative passes, known to cross floodplains. The seasonal flooding dynamics are clearly visible at all three evaluated floodplains. Darker blue colors indicate higher water occurrence. The tracks in Fig. 12 correspond to track 498 (descending) and 85 (ascending) in Fig. 13. It is interesting to note the drought in 2019, which is clearly visible in all three wetlands, particularly at the Sentinel-3A VS on track 741, which appears to suggest the level has remained 2m below the mean well into the 2019-2020 wet season. It is interesting to note that there are several valuable observations along Sentinel-3B ground track 498, although the water occurrence is 0%. This is likely due to the frequent cloud cover over the floodplain. The datasets also hold valuable information regarding slope in the wetland. This is a particular feature of the orientation of the wetland compared to the satellite tracks, which creates a spatially dense sampling pattern along the river line and floodplain. This could be useful in hydrologic/hydrodynamic modelling of the river in the region.
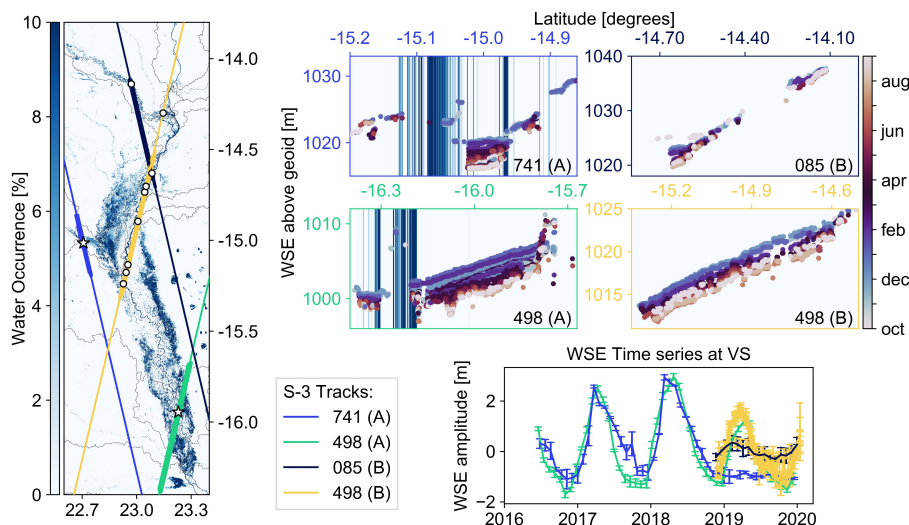
Figure 13. Floodplain dynamics in the Barotse floodplain as observed by Sentinel-3A (ground track 741 and 498) and Sentinel-3B (ground track 85 and 498). The WSE cross-sections are in order of crossing tracks from West to East. The cyclical color scheme shows the WSE amplitude over the hydrological year. The line colors in the time series correspond to the track colors from the map and the width of the line indicates the observations shown in the scatter plots. The error bars reflect the standard deviation for each pass used in the time series. The water occurrence thresholds are deliberately set from to 0-10% to enable the visualization of the floodplain.

In the Kafue Flats, we see seasonal patterns, with high flow occurring in spring and low flow starting in the late summer (Fig. 14). We also see gradual smoothing in the WSE time series as the distance to the Itezhi-Tezhi reservoir upstream decreases. The
395 upstream WSE is driven by reservoir release with sharp changes in WSE, whereas wetland processes smooth the downstream WSE. There are no valid VS on the tributaries located very close to frequently flooded areas (Sentinel-3B track 298 and Sentinel-3A track 541). The time series at the VS on Sentinel-3A track 070 and Sentinel-3B track 184 both present a sharp increase in January 2019 followed by a sharp return to the previously low level. The pass standard deviation is also larger in the upstream part. The tracks are both in the upstream part of the wetland, with nearby seasonally flooded areas. Both findings
400 are coherent with the results from Jiang et al. (2020), which identified nearby bright targets such as small lakes and ponds as a key source of errors for Sentinel-3. In this case, there are either no observations or unlikely artefacts in the time series.
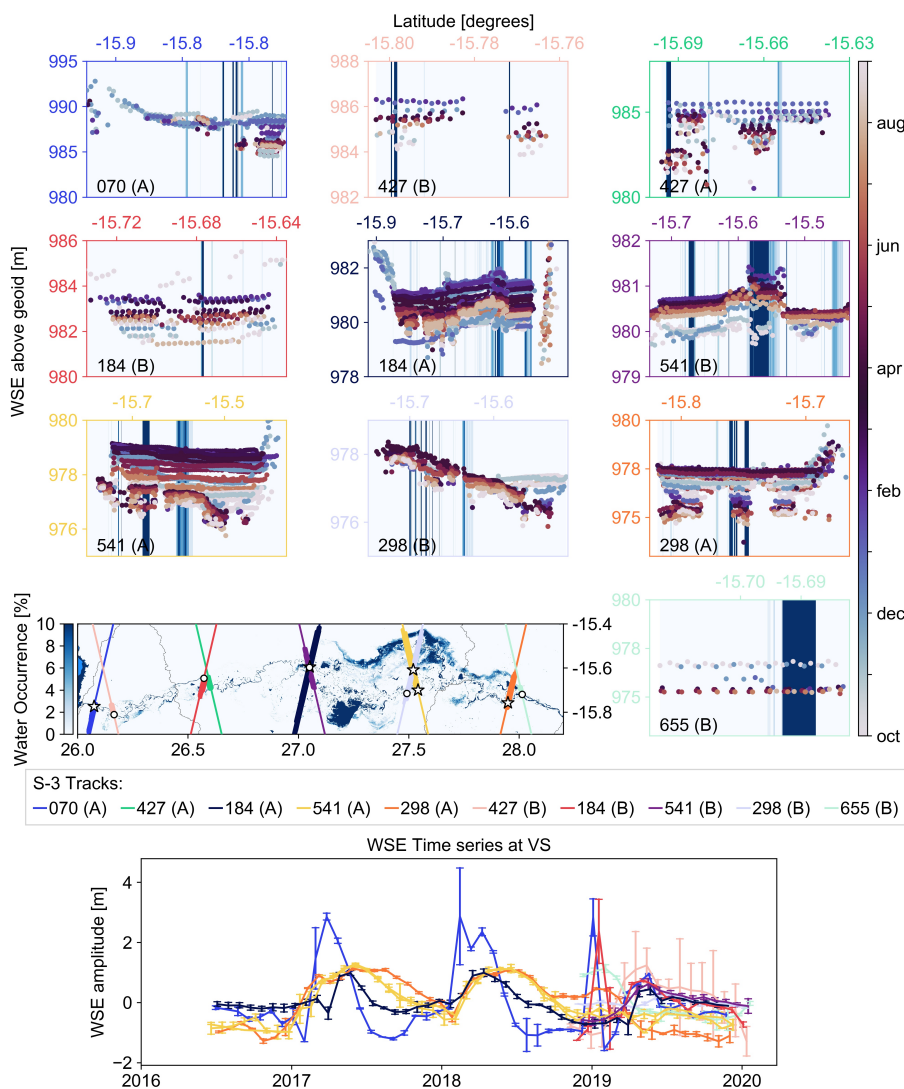
Figure 14. Floodplain dynamics in the Kafue Flats as observed by Sentinel-3A and Sentinel-3B. The tracks are ordered by longitude moving left to right on the map. The WSE cross-sections are in order of crossing tracks from West to East. The line colors in the time series correspond to the track colors from the map and the width of the line indicates the observations shown in the scatter plots. The frame colors and line colors in the time series correspond to the track colors from the map. The error bars reflect the standard deviation for each pass used in the time series. The water occurrence thresholds are deliberately set from to 0-10% to enable the visualization of the floodplain.

The WSE in the Chobe region reflect the dry 2019 wet season – the peak WSE is lower than the previous two years on record (Fig. 15). We see two different behaviors at the VS in the wetland region. In the Southern portion, prior to confluence with the Zambezi River, the amplitude is smaller. The wet season is slightly delayed with a more gradual decrease after the peak WSE height; however, in winter 2019-2020, the level has continued to decrease, as seen at all VS in the region. On the

405

Zambezi, the annual amplitude is closer to 5m and there is a clear attenuation in the maximum water level in the 2019-2020 season compared to previous years. This was clear at station 3045 in Figure 6 as well compared to records from 2000-2010.
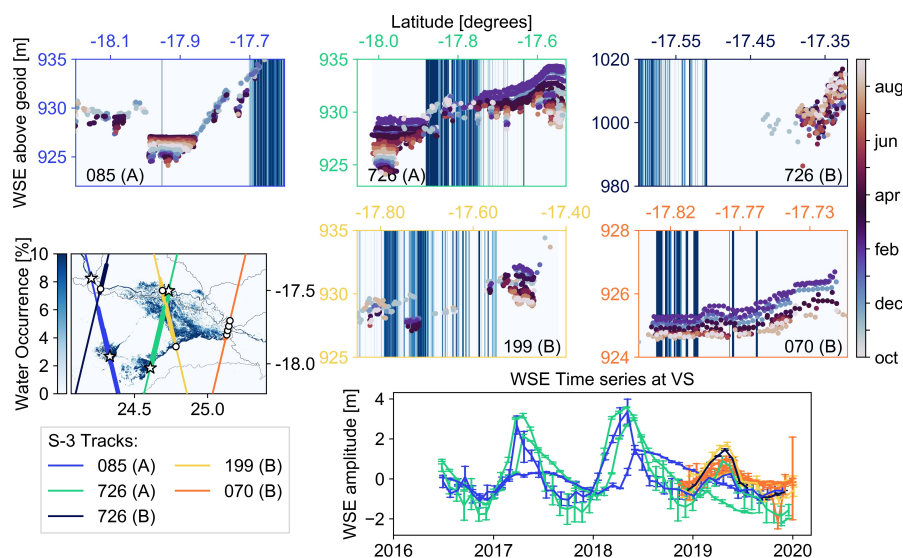
Figure 15. Floodplain dynamics in Chobe as observed by Sentinel-3A (left) and Sentinel-3B (right). The WSE cross-sections are in order of crossing tracks from West to East. The cyclical color scheme shows the WSE amplitude over the hydrological year. The line colors in the time series correspond to the track colors from the map and the width of the line indicates the observations shown in the scatter plots. The error bars reflect the standard deviation for each pass used in the time series. The water occurrence thresholds are deliberately set from to 0-10% to enable the visualization of the floodplain.

4.4 Perspectives

This study explores the potential for extracting Sentinel-3 WSE at catchment-level. The perspectives are two-fold. First, we
410 present a dense monitoring network for the Zambezi basin, with high spatial coverage and monthly observations of WSE. Satellite observations of WSE have been used in several studies to obtain information on river dynamics and to calibrate and update hydrological models (Domeneghetti, 2016; Dubey et al., 2015; Finsen et al., 2014; Schneider et al., 2018a). Schneider et al. (2018b) and Jiang et al. (2019b) have explored the value of high spatial resolution in calibrating hydrodynamic model parameters by using altimetry WSE observations. Jiang et al. (2019b) evaluated the value of calibrating with different spatio-
415 temporal densities and their results reveal a high benefit from the high spatial distribution of CryoSat-2 and Envisat observations as opposed to the Jason missions. The Sentinel-3 orbit is similar to the Envisat orbit to provide continuity; therefore, we expect similar results from the integration of Sentinel-3 WSE observations in a similar setup. Furthermore, calibration and assimilation approaches created for CryoSat-2 can also be applied where Sentinel-3 runs parallel to the river line.

The availability of in-situ records is limited relative to the catchment size. Although the performance of the Sentinel-3

420 satellites cannot be fully validated in the entire catchment, previous studies confirm the performance observed in this study (Jiang et al., 2020). The potential value of altimetry VS is high in poorly gauged catchments and subcatchments, where altimetry may be the only source of water level observations.

Furthermore, we show that Sentinel-3 can be used to provide spatio-temporal characterization of floodplains, as clear seasonal patterns can be seen where the satellite crosses wetlands and floodplains. The connectivity between river and floodplains

425 is an important hydrogeomorphic process, which can significantly alter the floodplain landscape. Park (2020) showed the potential in using satellite altimetry for this purpose using Jason-2 WSE in the Amazon. The results from this study suggest that Sentinel-3 may be an interesting candidate for similar studies due to the closer ground-track spacing and reduced footprint from the SAR altimeter.

The cross-sections extracted over floodplains are similar to observations expected from the future SWOT (Surface Water

430 and Ocean Topography) mission (Domeneghetti et al., 2018). Amongst other variables, observations of WSE, water extent and slope are expected from SWOT. Another novel dataset will be 2-dimensional observations of WSE and water extent within two 50-km wide swaths. Similar information can already be extracted from the Sentinel-3 dataset in selected locations. SWOT is expected to be launched in 2021; therefore, the Sentinel-3 dataset represents a highly valuable source of information and training datasets.

435 ## 5 Conclusions

Satellite radar altimetry has been widely used in the past decades to bridge the gap between data requirements in hydrologic/hydrodynamic simulations and in-situ data availability. In this study, we explore the capabilities of Sentinel-3 to provide catchment-scale WSE observations for monitoring purposes. The network can be used to supplement limited in-situ records for monitoring applications and to inform hydrologic/hydrodynamic models. The dual satellite mission Sentinel-3 joins a new

440 generation of satellites carrying high-resolution SAR altimeters. It is the first mission in a near-polar orbit to carry SAR altimeters and use open-loop tracking. The open-loop tracking mode should improve the positioning of the altimeter range window over narrow targets or rugged topography, e.g. several rivers, where the surface elevation is known.

In this study we have extracted all Sentinel-3A and Sentinel-3B virtual station datasets over the Zambezi river basin in Africa at processing level 1B and 2 and developed an automatic workflow to remove outliers, retaining only clear water targets and

445 provide reliable WSE at all possible locations in the basin. We extract over 360 virtual stations from each satellite of which over 70 are validated based on the waveforms and temporal coverage for each Sentinel-3 satellite. The proposed approach more than triples the number of VS compared to the global database Hydroweb. Where in-situ gauging stations are available, the RMSD is less than 32 cm. We show that a dense, Sentinel-3 monitoring network can be extracted at catchment scale, using global datasets and publicly available processing tools. The dataset can be used to monitor river WSE and river-floodplain

450 interactions. In particular, we see significant potential for wetlands parallel to satellite tracks, e.g. the Barotse floodplain in the Zambezi.

In addition, the upgrade of the OLTC on board Sentinel-3A directly increased the number of VS. Thus, higher coverage can be attained when adequate targets are defined on board. Surprisingly, we note that the GPOD-processed data fails at several VS, although the dataset produces more robust data overall. Analysis links one source of the problem to the L1b
455 processing and open-loop tracking mode. Increasing the receiving window appears to mitigate this, making the option highly relevant on the GPOD platform, as more targets can be successfully processed. While the open-loop mode combined with the high-resolution SAR altimeter provides clear advantages in processing narrow targets, the sharp changes in reception window position introduced by the on board pseudo-DEM can have similar impacts as sharp changes in topography.

Appendix A: Supplementary information on VS location
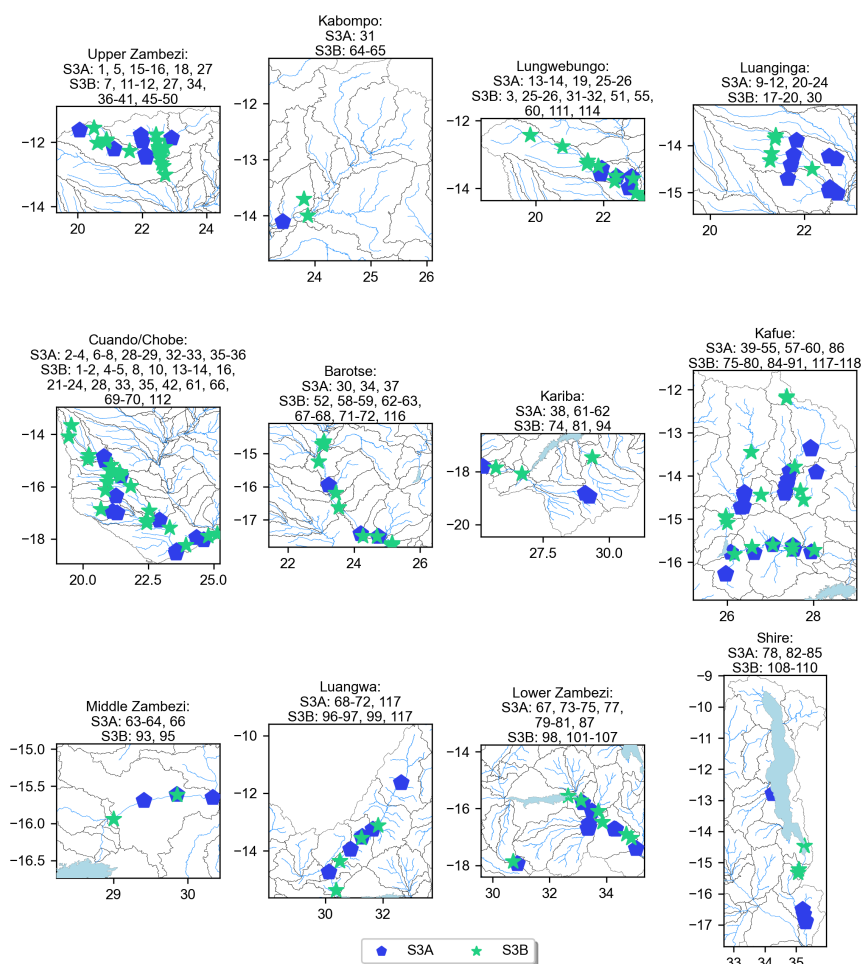
Figure A1. All Sentinel-3 VS considered in this study.
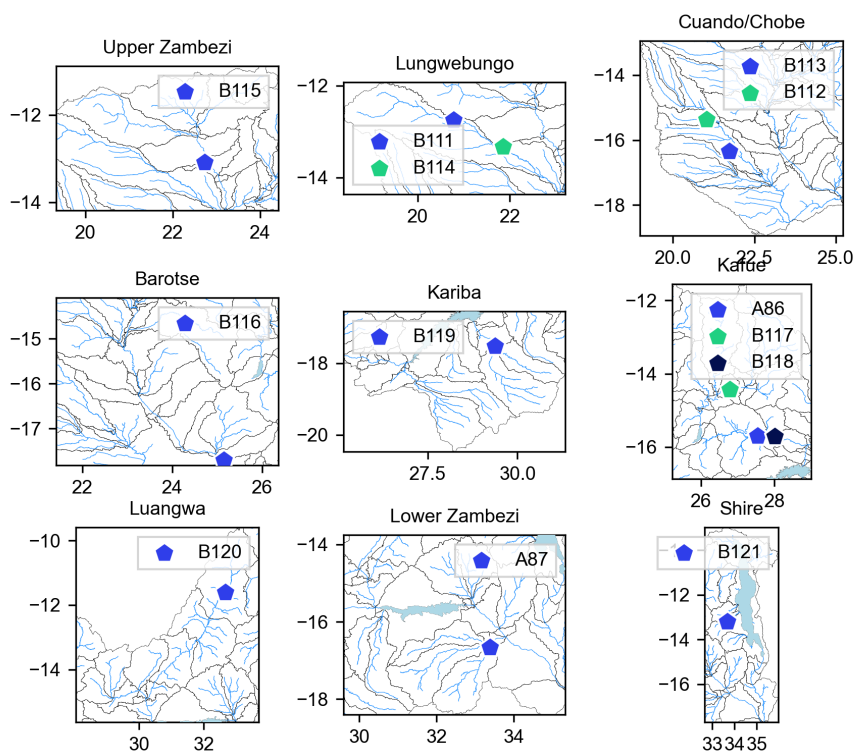
Figure B1. S3A and S3B VS improved by the 3x window extension in the GPOD processing options and outperforming SciHub as a result.
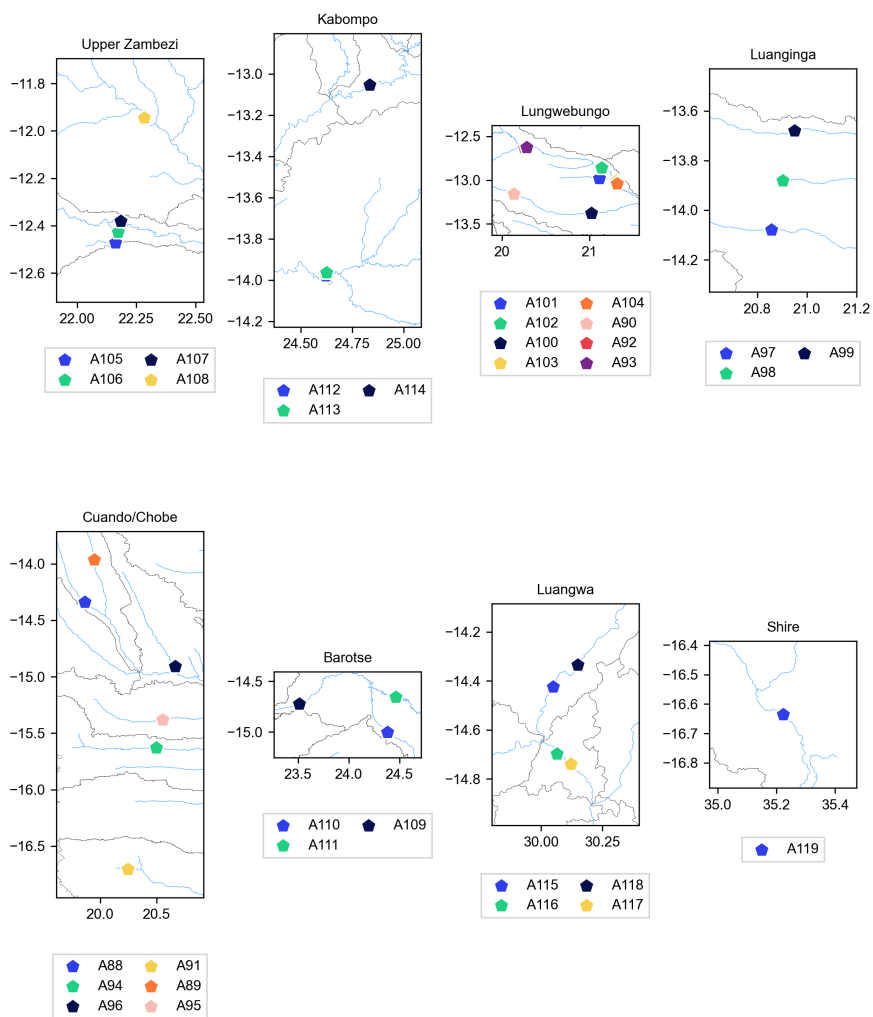
Figure C1. Sentinel-3A VS improved by the OLTC update in the GPOD and SciHub datasets.

460 *Author contributions.* Cécile M. M. Kittel and developed the methodology and code with inputs from Liguang Jiang. The work was supervised by Peter Bauer-Gottwein and Christian Tøttrup. Cécile M. M. Kittel prepared the manuscript including the figures and tables with contributions from all the co-authors.

Competing interests. The authors declare that they have no conflict of interest

Acknowledgements. This work has been conducted in the context of the European Space Agency (ESA) project Earth Observations for

465 Sustainable Development (EO4SD, contract number 4000117094/16/I-NB). The authors wish to thank the Zambezi River Authority (ZRA) for providing in-situ water level observations. We would like to acknowledge Salvatore Dinardo for his assistance on the GPOD/SARvatore service.

References

Abiodun, B. J., Makhanya, N., Petja, B., Abatan, A. A., and Oguntunde, P. G.: Future projection of droughts over major river basins in Southern Africa at specific global warming levels, Theoretical and Applied Climatology, 137, 1785–1799, https://doi.org/10.1007/s00704-018-2693-0, 2019.

Arsen, A., Crétaux, J. F., and Abarca del Rio, R.: Use of SARAL/AltiKa over Mountainous Lakes, Intercomparison with Envisat Mission, Marine Geodesy, 38, 534–548, https://doi.org/10.1080/01490419.2014.1002590, 2015.

Beilfuss, R.: A Risky Climate for Southern African Hydro: Assessing Hydrological Risks and Consequences for Zambezi River Basin Dams, International Rivers, pp. 1–60, https://doi.org/10.13140/RG.2.2.30193.48486, 2012.

Berry, P. A. M., Garlick, J. D., Freeman, J. A., and Mathers, E. L.: Global inland water monitoring from multi-mission altimetry, Geophysical Research Letters, 32, 1–4, https://doi.org/10.1029/2005GL022814, 2005.

Biancamaria, S., Schaedele, T., Blumstein, D., Frappart, F., Boy, F., Desjonquères, J. D., Pottier, C., Blarel, F., and Niño, F.: Validation of Jason-3 tracking modes over French rivers, Remote Sensing of Environment, 209, 77–89, https://doi.org/10.1016/j.rse.2018.02.037, 2018.

Boergens, E., Buhl, S., Dettmering, D., Klüppelberg, C., and Seitz, F.: Combination of multi-mission altimetry data along the Mekong River with spatio-temporal kriging, Journal of Geodesy, 91, 519–534, https://doi.org/10.1007/s00190-016-0980-z, 2017.

Crétaux, J. F., Jelinski, W., Calmant, S., Kouraev, A., Vuglinski, V., Bergé-Nguyen, M., Gennero, M. C., Nino, F., Abarca Del Rio, R., Cazenave, A., and Maisongrande, P.: SOLS: A lake database to monitor in the Near Real Time water level and storage variations from remote sensing data, Advances in Space Research, 47, 1497–1507, https://doi.org/10.1016/j.asr.2011.01.004, 2011.

Dinardo, S., Fenoglio-Marc, L., Buchhaupt, C., Becker, M., Scharroo, R., Joana Fernandes, M., and Benveniste, J.: Coastal SAR and PLRM altimetry in German Bight and West Baltic Sea, Advances in Space Research, 62, 1371–1404, https://doi.org/10.1016/j.asr.2017.12.018, 2018.

Domeneghetti, A.: On the use of SRTM and altimetry data for flood modeling in data-sparse regions, Water Resources Research, 52, 2901–2918, https://doi.org/doi:10.1002/2015WR017967, 2016.

Domeneghetti, A., Tarpanelli, A., Brocca, L., Barbetta, S., Moramarco, T., Castellarin, A., and Brath, A.: The use of remote sensing-derived water surface data for hydraulic model calibration, Remote Sensing of Environment, 149, 130–141, https://doi.org/10.1016/j.rse.2014.04.007, 2014.

Domeneghetti, A., Schumann, G. J., Frasson, R. P., Wei, R., Pavelsky, T. M., Castellarin, A., Brath, A., and Durand, M. T.: Characterizing water surface elevation under different flow conditions for the upcoming SWOT mission, Journal of Hydrology, 561, 848–861, https://doi.org/10.1016/j.jhydrol.2018.04.046, 2018.

Dubey, A. K., Gupta, P. K., Dutta, S., and Singh, R. P.: An improved methodology to estimate river stage and discharge using Jason-2 satellite data, Journal of Hydrology, 529, 1776–1787, https://doi.org/10.1016/j.jhydrol.2015.08.009, 2015.

Finsen, F., Milzow, C., Smith, R., Berry, P., and Bauer-Gottwein, P.: Using radar altimetry to update a large-scale hydrological model of the Brahmaputra river basin Flemming Finsen , Christian Milzow , Richard Smith , Philippa Berry, Hydrology Research, 45, 148–164, https://doi.org/10.2166/nh.2013.191, 2014.

Getirana, A. C. V. and Peters-Lidard, C.: Estimating water discharge from large radar altimetry datasets, Hydrology and Earth System Sciences, 17, 923–933, https://doi.org/10.5194/hess-17-923-2013, 2013.

Hannah, D. M., Demuth, S., van Lanen, H. A., Looser, U., Prudhomme, C., Rees, G., Stahl, K., and Tallaksen, L. M.: Large-scale river flow archives: Importance, current status and future needs, Hydrological Processes, 25, 1191–1200, https://doi.org/10.1002/hyp.7794, 2011.

505 Jain, M.: Improved sea level determination in the Arctic regions through development of tolerant altimetry retracking, Phd thesis, Technical University of Denmark (DTU), 2015.

Jiang, L., Nielsen, K., Andersen, O. B., and Bauer-Gottwein, P.: Monitoring recent lake level variations on the Tibetan Plateau using CryoSat-2 SARIn mode data, Journal of Hydrology, 544, 109–124, https://doi.org/10.1016/j.jhydrol.2016.11.024, http://dx.doi.org/10.1016/j.jhydrol.2016.11.024, 2017a.

510 Jiang, L., Nielsen, K., Andersen, O. B., and Bauer-Gottwein, P.: CryoSat-2 radar altimetry for monitoring freshwater resources of China, Remote Sensing of Environment, 200, 125–139, https://doi.org/10.1016/j.rse.2017.08.015, 2017b.

Jiang, L., Baltazar, O., Nielsen, K., Zhang, G., and Bauer-gottwein, P.: Remote Sensing of Environment Influence of local geoid variation on water surface elevation estimates derived from multi-mission altimetry for Lake Namco, Remote Sensing of Environment, 221, 65–79, https://doi.org/10.1016/j.rse.2018.11.004, 2019a.

515 Jiang, L., Madsen, H., and Bauer-Gottwein, P.: Simultaneous calibration of multiple hydrodynamic model parameters using satellite altimetry observations of water surface elevation in the Songhua River, Remote Sensing of Environment, 225, 229–247, https://doi.org/10.1016/j.rse.2019.03.014, 2019b.

Jiang, L., Nielsen, K., Dinardo, S., Andersen, O. B., and Bauer-Gottwein, P.: Evaluation of Sentinel-3 SRAL SAR altimetry over Chinese rivers, Remote Sensing of Environment, 237, 111 546, https://doi.org/https://doi.org/10.1016/j.rse.2019.111546, 2020.

520 Kittel, C. M. M., Nielsen, K., Tøttrup, C., and Bauer-Gottwein, P.: Informing a hydrological model of the Ogooué with multi-mission remote sensing data, Hydrology and Earth System Sciences, 22, 1453–1472, https://doi.org/10.5194/hess-22-1453-2018, 2018.

Kleinherenbrink, M., Lindenbergh, R. C., and Ditmar, P. G.: Monitoring of lake level changes on the Tibetan Plateau and Tian Shan by retracking Cryosat SARIn waveforms, Journal of Hydrology, 521, 119–131, https://doi.org/10.1016/j.jhydrol.2014.11.063, 2015.

Liu, G., Schwartz, F. W., Tseng, K.-H., and Shum, C. K.: Discharge and water-depth estimates for ungauged rivers: Combining hydrologic, 525 hydraulic, and inverse modeling with stage and water-area measurements from satellites, Water Resouces Research, 51, 6017–6035, https://doi.org/10.1002/2015WR017200.A, 2015.

Michailovsky, C. I. and Bauer-Gottwein, P.: Operational reservoir inflow forecasting with radar altimetry: the Zambezi case study, Hydrol. Earth Syst. Sci., 18, 997–1007, https://doi.org/10.5194/hess-18-997-2014, 2014.

Michailovsky, C. I., McEnnis, S., Berry, P. a. M., Smith, R., and Bauer-Gottwein, P.: River monitoring from satellite radar altimetry in the 530 Zambezi River basin, Hydrology and Earth System Sciences, 16, 2181–2192, https://doi.org/10.5194/hess-16-2181-2012, 2012.

Michailovsky, C. I., Milzow, C., and Bauer-Gottwein, P.: Assimilation of radar altimetry to a routing model of the Brahmaputra River, Water Resources Research, 49, 4807–4816, https://doi.org/10.1002/wrcr.20345, 2013.

Myers, E., Hess, K., Yang, Z., Xu, J., Wong, A., Doyle, D., Woolard, J., White, S., Le, B., Gill, S., and Hovis, G.: VDatum and strategies for national coverage, Oceans Conference Record (IEEE), https://doi.org/10.1109/OCEANS.2007.4449348, 2007.

535 Nielsen, K., Stenseng, L., Andersen, O. B., and Knudsen, P.: The performance and potentials of the CryoSat-2 SAR and SARIn modes for lake level estimation, Water (Switzerland), 9, https://doi.org/10.3390/w9060374, 2017.

Park, E.: Remote Sensing of Environment Characterizing channel- floodplain connectivity using satellite altimetry : Mechanism , hydro-geomorphic control , and sediment budget, Remote Sensing of Environment, 243, 111 783, https://doi.org/10.1016/j.rse.2020.111783, https://doi.org/10.1016/j.rse.2020.111783, 2020.

540 Pekel, J.-F., Cottam, A., Gorelick, N., and Belward, A. S.: High-resolution mapping of global surface water and its long-term changes, Nature, 540, 418–422, https://doi.org/10.1038/nature20584, http://www.nature.com/doifinder/10.1038/nature20584, 2016.

Rosmorduc, V.: Hydroweb Product User Manual V1.0, 2016.

Roux, E., Santos da Silva, J., Cesar Vieira Getirana, A., Bonnet, M.-P., Calmant, S., Martinez, J.-M., and Seyler, F.: Producing time series of river water height by means of satellite radar altimetry—a comparative study, Hydrological Sciences Journal, 55, 104–120, https://doi.org/10.1080/02626660903529023, 2010.

Schneider, R., Godiksen, P. N., Villadsen, H., Madsen, H., and Bauer-Gottwein, P.: Application of CryoSat-2 altimetry data for river analysis and modelling, Hydrology and Earth System Sciences, 21, 751–764, https://doi.org/10.5194/hess-21-751-2017, 2017.

Schneider, R., Ridler, M. E., Godiksen, P. N., Madsen, H., and Bauer-Gottwein, P.: A data assimilation system combining CryoSat-2 data and hydrodynamic river models, Journal of Hydrology, 557, 197–210, https://doi.org/10.1016/j.jhydrol.2017.11.052, 2018a.

Schneider, R., Tarpanelli, A., Nielsen, K., Madsen, H., and Bauer-Gottwein, P.: Evaluation of multi-mode CryoSat-2 altimetry data over the Po River against in situ data and a hydrodynamic model, Advances in Water Resources, 112, 17–26, https://doi.org/10.1016/j.advwatres.2017.11.027, 2018b.

Schwatke, C., Dettmering, D., Bosch, W., and Seitz, F.: DAHITI - An innovative approach for estimating water level time series over inland waters using multi-mission satellite altimetry, Hydrology and Earth System Sciences, 19, 4345–4364, https://doi.org/10.5194/hess-19-4345-2015, 2015.

Tarpanelli, A., Amarnath, G., Brocca, L., Massari, C., and Moramarco, T.: Discharge estimation and forecasting by MODIS and altimetry data in Niger-Benue River, Remote Sensing of Environment, 195, 96–106, https://doi.org/10.1016/j.rse.2017.04.015, 2017.

Villadsen, H., Andersen, O. B., Stenseng, L., Nielsen, K., and Knudsen, P.: CryoSat-2 altimetry for river level monitoring — Evaluation in the Ganges–Brahmaputra River basin, Remote Sensing of Environment, 168, 80–89, https://doi.org/10.1016/j.rse.2015.05.025, 2015.

Villadsen, H., Deng, X., Andersen, O. B., Stenseng, L., Nielsen, K., and Knudsen, P.: Improved inland water levels from SAR altimetry using novel empirical and physical retrackers, Journal of Hydrology, 537, 234–247, https://doi.org/10.1016/j.jhydrol.2016.03.051, 2016.

Vörösmarty, C., Askew, A., Grabs, W., Barry, R. G., Birkett, C., Döll, P., Goodison, B., Hall, A., Jenne, R., Kitaev, L., Landwehr, J., Keeler, M., Leavesley, G., Schaake, J., Strzepek, K., Sundarvel, S. S., Takeuchi, K., and Webster, F.: Global water data: A newly endangered species, Eos, 82, 54–58, https://doi.org/10.1029/01EO00031, 2001.

Vu, P. L., Frappart, F., Darrozes, J., Marieu, V., Blarel, F., Ramillien, G., Bonnefond, P., and Birol, F.: Multi-satellite altimeter validation along the French Atlantic coast in the southern Bay of Biscay from ERS-2 to SARAL, Remote Sensing, 10, https://doi.org/10.3390/rs10010093, 2018.

Wingham, D. J., Francis, C. R., Baker, S., Bouzinac, C., Brockley, D., Cullen, R., de Chateau-Thierry, P., Laxon, S. W., Mallow, U., Mavrocordatos, C., Phalippou, L., Ratier, G., Rey, L., Rostan, F., Viau, P., and Wallis, D. W.: CryoSat: A mission to determine the fluctuations in Earth's land and marine ice fields, Advances in Space Research, 37, 841–871, https://doi.org/10.1016/j.asr.2005.07.027, 2006.

Yamakazi, D., Ikeshima, D., Tawatari, R., Yamaguchi, T., O'Loughlin, F., Neal, J. C., Sampson, C. C., Kanae, S., and Bates, P. D.: A high-accuracy map of global terrain elevations Dai, Geophysical Research Letters, 44, 5844–5853, https://doi.org/10.1002/2017GL072874, 2017.

Yan, D., Wang, K., Qin, T., Weng, B., Wang, H., Bi, W., Li, X., Li, M., Lv, Z., Liu, F., He, S., Ma, J., Shen, Z., Wang, J., Bai, H., Man, Z., Sun, C., Liu, M., Shi, X., Jing, L., Sun, R., Cao, S., Hao, C., Wang, L., Pei, M., Dorjsuren, B., Gedefaw, M., Girma, A., and Abiyu, A.: A data set of global river networks and corresponding water resources zones divisions, Scientific data, 6, 219, https://doi.org/10.1038/s41597-019-0243-y, 2019.